Beef muscle discrimination based on two-trace two-dimensional correlation spectroscopy (2T2D COS) combined with snapshot visible-near infrared multispectral imaging

Abderrahmane Aït-Kaddour, Mohammed Loudiyi, Oumayma Boukria, Jasur Safarov, Shaxnoza Sultanova, Donato Andueza, Anne Listrat, Yana Cahyana

HAL Id: hal-04582563

https://hal.inrae.fr/hal-04582563

Submitted on 22 May 2024

Beef muscle discrimination based on two-trace two-dimensional correlation spectroscopy (2T2D COS) combined with snapshot visible-near infrared multispectral imaging

Abderrahmane Aït-Kaddour [a,f,*], Mohammed Loudiyi [a], Oumayma Boukria [b], Jasur Safarov [c], Shaxnoza Sultanova [d], Donato Andueza [e], Anne Listrat [e], Yana Cahyana [f]

[a] *Université Clermont Auvergne, INRAE, VetAgro Sup, UMRF, Lempdes F-63370, France*
[b] *Applied Organic Chemistry Laboratory, Sciences and Techniques Faculty, Sidi Mohamed Ben Abedallah University, BP 2202 route d'Immouzer, Fès, Morocco*
[c] *Department of Food Engineering, Faculty of Mechanical Building, Tashkent State Technical University named after Islam Karimov, University Str. 2, Tashkent 100095, Uzbekistan*
[d] *Joint Belarusian-Uzbek Intersectoral Institute of Applied Technical Qualifications in Tashkent, 111200, Tashkent region, Kibray district, Koramurt street, 1, Uzbekistan*
[e] *Université Clermont Auvergne, INRAE, VetAgro Sup, UMR Herbivores, Saint-Genès-Champanelle F-63122, France*
[f] *Laboratory of Food Chemistry, Department of Food Technology, Universitas Padjadjaran, Bandung, Indonesia*

A R T I C L E I N F O	A B S T R A C T
	The purpose of this work was to assess the potential of 2T2D COS PLS-DA (two-trace two-dimensional correlation spectroscopy and partial least squares discriminant analysis) in conjunction with Visible Near infrared multi-spectral imaging (MSI) as a quick, non-destructive, and precise technique for classifying three beef muscles -*Longissimus thoracis, Semimembranosus,* and *Biceps femoris*- obtained from three breeds - the Blonde d'Aquitaine, Limousine, and Aberdeen Angus. The experiment was performed on 240 muscle samples. Before performing PLS-DA, spectra were extracted from MSI images and processed by SNV (Standard Normal Variate), MSC (Multivariate Scattering Correction) or AREA (area under curve equal 1) and converted in synchronous and asynchronous 2T2D COS maps. The results of the study highlighted that combining synchronous and asynchronous 2T2D COS maps before performing PLS-DA was the best strategy to discriminate between the three muscles (100% of classification accuracy and 0% of error).

1. Introduction

Food products' authenticity and traceability are crucial because they guarantee fair trade practices, food safety, and consumer confidence in the agro-food chain. They are also very important, especially for special diets (allergy, health, etc.) or religious beliefs (Islam, Judaism, Hinduism, etc.). Amongst food products, meat authenticity is crucial due to the prevalence of product falsification and adulteration as observed in the past few decades (e.g. horse gate, bovine spongiform encephalopathy) (Rao, Chakraborty, & Murthy, 2019). Given the growing incidence of mislabeling, it is imperative that beef makers have a mechanism to verify meat products. In 2017, the meat speciation segment accounted for one-third share of the global market authenticity testing (Rao et al., 2019). According to Listrat et al. (2020) the quality of meat is associated to its chemical composition. However, the final muscle quality (such as

juiciness and tenderness) can be greatly influenced by the type of muscle and the breed of animal from which the muscle is obtained. Achieving discrimination of raw pieces and of the animal breed is therefore important due to the increase of the substitution of higher quality meat pieces by lower quality ones (Cozzolino & Murray, 2004).

There are several conventional laboratory-based procedures available for analyzing meat and determining its quality. For example, physicochemical parameters like pH, water activity, moisture, protein, lipid content, tenderness, and freshness (Nache, Scheier, Schmidt, & Hitzmann, 2015; Pérez-Palacios et al., 2017; Tao, Peng, Li, Chao, & Dhakal, 2012; Wei, Peng, Li, & Qiao, 2015) can be used to evaluate meat quality. Nevertheless, those methods are time-consuming and harmful for some of them, which prevents regular application in step with industry production rates. Technologies that meet the requirements and criteria of the industrial world have recently emerged. Typically,

---

spectroscopy serves as their foundation. Both spectrum imaging (multispectral, hyperspectral, and microscopy) and classical spectroscopic techniques (fluorescence, infrared, near-infrared, Raman, and laser-induced breakdown) have been applied in research and industry for various reasons such as quick and non-destructive evaluation of food chemical composition (Kamruzzaman, ElMasry, Sun, & Allen, 2012; Prieto, Andrés, Giráldez, Mantecón, & Lavín, 2006), microbiological safety (Moreirinha, Nunes, Barros, Almeida, & Delgadillo, 2015), authentication (Casale, Casolino, Ferrari, & Forina, 2008; S. S. Kim, Rhyu, Kim, & Lee, 2003), and process analytical technology (Gowen, O'Donnell, Cullen, Downey, & Frias, 2007). The various characteristics of meat samples, such as moisture, fat, tenderness, color, water-holding capacity, pH, and microbial decomposition are typically assessed using MSI (multispectral imaging) and HSI (hyperspectral imaging) techniques (Feng, Makino, Oshita, & Martín, 2018).

In terms of muscle type classification, four lamb muscle types (Longissimus Dorsi, Psoas Major, Semimembranosus, and Semitendinosus) have been classified using HSI in the 380–1028 nm wavelength range (Sanz et al., 2016). The best classification findings in this investigation were obtained by the authors utilizing Least Mean Squares (LSM) with a 96.67% classification accuracy. In a similar vein, Aït-Kaddour, Jacquot, Micol, and Listrat (2017) employed a MSI outfitted with nineteen Light emitting Diodes (450 to 1050 nm) to distinguish three beef meat muscles (Longissimus thoracis, Biceps femoris, and Semimembranosus) according to their respective muscle categories and animal origins. The results of PLS-DA (partial least square discriminant analysis) indicated a range of 63.5 to 83% for accurate classification. In the study of Sanz et al. (2016) seven classifier were used, LMS (Linear Least Mean Squares Algorithm), MLP-SGG (Multi-Layer Perceptron with Scaled Conjugate Gradient), υ-SVM (Scholkopf's Support Vector Machines algorithm), SMO (Platt's Sequential Minimal Optimization Algorithm Standard Normal Variate -SNV-), LR (Logistic Regression), CentreNN (Centre based nearest Neighbor classifier) and LDA (Linear Discriminant Analysis) coupled or not with PCA to reduce the dimensionality of the initial data. The best classification accuracy of the previously mentioned classifiers was 96.67, 95, 85.83, 90.83, 91.67, and 85.83% respectively without PCA preprocessing. The last classifier, LDA, provided no results for classification certainly due to sample features and the quantity of cases utilized during the study learning process. In the study of Aït-Kaddour et al. (2017), three preprocessing techniques were applied to image mean spectra (reduction of the area under the spectra to a value of 1 -AREA-, Multiple scattering correction-MSC-, and SNV) before performing muscle classification by PLS-DA. They reported that nearly all discrimination models calculated with preprocessed data were more parsimonious (i.e. needed less factors of regression) and that the best model was obtained after applying AREA correction to spectra. The two studies, discussed above, reported their best results for classification (accuracy = 96.67 and 83%), after investigating various chemometrics or data transformation techniques. As a result, it can be concluded that attaining a high classification accuracy for animal muscles is difficult and directly relates to the algorithm used to create discrimination models as well as the data preprocessing technique (Sanz et al., 2016).

Two-Trace Two-dimensional Correlation Spectroscopy, or 2T2D COS as it is commonly known, is a novel approach to sample comparison that is making its way through the scientific literature (Noda, 2018). This approach uses 2D COS techniques (Noda, 1993) to distinguish the weak signals variation of two spectra submitted to an external perturbation. It is typically used to compare a pair of spectra. This method works well for identifying variations between overlapping peaks. As a result, the 2T2D COS approach typically yields a wealth of valuable characteristic information. In particular, this strategy has not been widely applied in food research to distinguish between different food samples. However, it might be a novel approach to data management, improving the accuracy of the model's discriminating.

This brief review of the literature demonstrates that few researches

has been done to address the issue of muscle type discrimination, particularly when employing the MSI technique. Furthermore, no research has been done to determine whether 2T2D COS analysis is relevant for differentiating between meat samples. In order to investigate the suitability of the multi-snapshot MSI system in conjunction with 2T2D COS as a quick, non-destructive method for classifying red meat according to muscle type, this present research was proposed.

2. Materials and methods

2.1. Beef production and muscle sampling

The study was carried out in compliance with French guidelines for the use of experimental animals, including animal welfare, as well as those of Animal Care and Use Committee of the National Institute for Agricultural Research (INRAE, Institut national de recherche pour l'agriculture, l'alimentation et l'environnement) of Clermont-Ferrand/Theix, France.

Forty young male cattle from three different animal types and three different breeds have been used in the experiment: Aberdeen Angus (AA; $n = 12$), Limousine (LI; $n = 14$), and Blonde d'Aquitaine (BA; n = 14). The conditions of production of animals were previously described by Dubost, Micol, Meunier, Lethias, and Listrat (2013). Animals were assigned to a 100-day finishing period. The animals were housed in straw bedded pens, individually fed and weighed every 2 weeks. Diets consisted of concentrate (75%) and straw (25%). The percentages of straw and concentrate were based on dry matter basis for daily diet weight. The animals with the weight of 670 kg or at 17 months on average were slaughtered at the INRAE Research Center's experimental slaughterhouse in Clermont-Ferrand/Theix, France. Three muscles (*Longissimus thoracis* [LT], *Semimembranosus* [SM], and *Biceps femoris* [BF], Fig. 1) were extracted from each animal carcasses in parallel to the direction of the muscle fibers in height, at the same localization inside each muscle (the 9th rib for LT and the center of SM and BF muscles). At 24 h' post-mortem, each muscle was removed from the carcass and chilled in a cold chamber. A total of 240 muscle samples were obtained by dividing the 120 muscles into two sections, each measuring 10 × 7 × 3 cm. One portion was vacuum packaged, immediately frozen in 100% ethanol and kept at −20 °C until MSI acquisition (120 muscle samples). The second portion (120 muscle samples) was aged for 14 days in vacuum packs. Muscle samples were kept at −20 °C until analysis and then frozen in pure ethanol after 14 days. A number of 240 samples of meat were collected at the conclusion of the trial. This was performed in order to increase the muscle variability and therefore the number of samples in the data base.

2.2. Muscle multispectral image acquisition

An MSI camera (Point Gray Research, Scorpion SCOR-20SOM, 1200 × 1200 pixels) equipped with a VideometerLab2® device (Videometer A/S, Denmark) was used to record the MSI of the 240 beef samples. The Videometer Lab2® is a Visible-Near Infrared (VIS-NIR) device commercialized with 19 emitting diodes at fixed wavelengths (405, 435, 450, 470, 505, 525, 590, 630, 645, 660, 700, 850, 870, 890, 910, 940, 950, 970, 1050 nm) (Aït-Kaddour et al., 2017). Prior to picture acquisition and to adjust the strobing time of each light emitting diode and prevent saturation, minimize shadows and shading effects the camera was calibrated using Videometer® standards for radiometric calibration (white and dark standard target plates) and geometric calibration (doted standard target plate), followed by a light setup based on the meat sample (Panagou, Papadopoulou, Carstensen, & Nychas, 2014). For each muscle and before image acquisition, the samples previously kept at −20 °C were thawed in their plastic bag at 4 °C, equilibrated at 20 °C in a water bath, and then cut gently into a 6 × 5 × 1.5 cm^3. The samples were wiped out with a paper towel to eliminate moisture on their surface. After that, the samples were placed in the dark by lowering the MSI
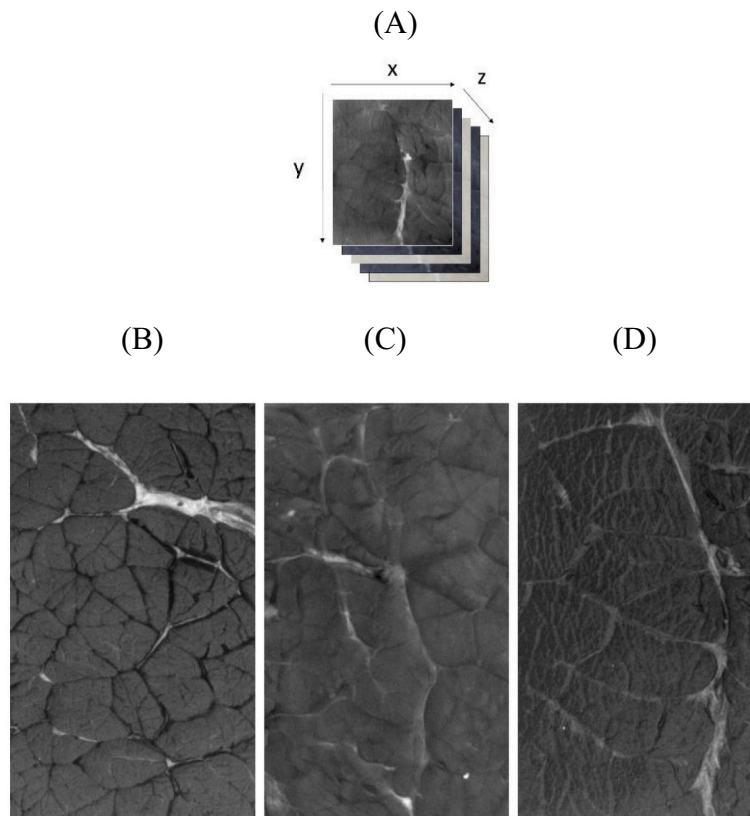
(A)

(B)   (C)   (D)

Fig. 1. (A) cube image of beef muscles (y = number of pixels in the y-axis; x = number of pixels in the x-axis, z = number of LEDs) recorded with the Videometer lab 2® device and Image of *Biceps femoris* (B), *Longissimus thoracis* (C) and *Semimembranosus* (D) muscles recorded after excitation at 405 nm for Limousine breed.

upper sphere. One image were recorded per muscle, representing 240 cube images for all the experiment (Fig. 1).

2.3. Image mean spectra

Using the image tools tab provided in the VideometerLab2® software, the mean multispectral image spectra were extracted manually from a fixed region of interest (ROI) of 700 × 575 pixels located at the center of each image. This was performed in order to prevent any side effect on recorded images (Fig. 2). Next, this ROI was then reproduced automatically on every MSI of meat samples. This made it possible to compile a database with the mean spectra of 4560 images (240 samples × 19 LEDs).

2.4. Preprocessing of image mean spectra

Three pre-processing techniques were applied to the mean MSI spectra of each image: SNV (Barnes, Bastian, Becker, & Martin, 1989), MSC (Aït-Kaddour et al., 2016), and normalization (AREA) (Aït-Kaddour et al., 2016). SNV correction is associated to a normalization of the spectra that consists in the subtraction of each spectrum by its own mean and dividing it by its own standard deviation (Sandak, Sandak, & Meder, 2016). After SNV, each spectrum will have a mean of 0 and a standard deviation of 1. The MSC method aims to correct spectra in such a way that they are as close as possible to a reference spectrum, the mean of the data set in the present study, by changing the scale and the offset of the spectra (Windig, Shaver, & Bro, 2008). Normalization (AREA = area under the spectral curve equal to 1) procedure scales the complete spectra so that these spectra represent the same overall concentration (Dieterle, Ross, Schlotterbeck, & Senn, 2006). The global goal of these techniques is to reduce the influence of non-targeted factors (light scattering, shifts in baseline, and non-linearity) and improve the signal-to-noise ratio.

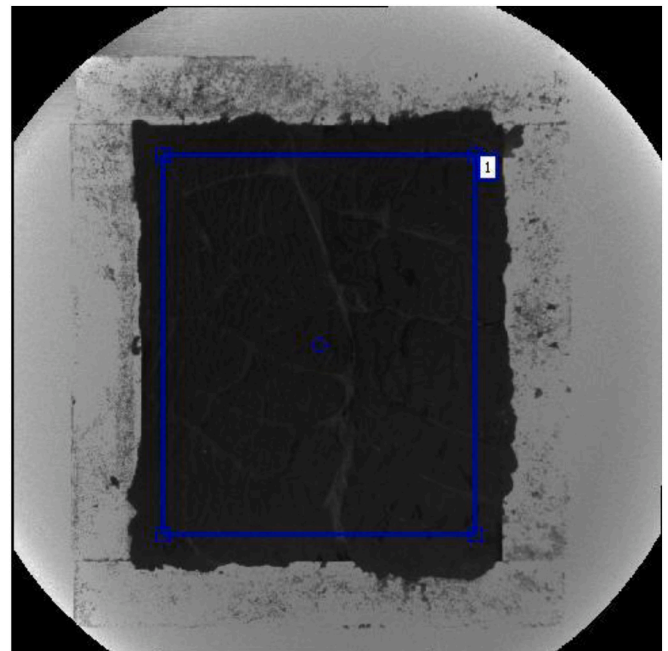**Fig. 2.** Image of beef muscle before extraction of the Region of Interest (blue square). (For interpretation of the references to color in this figure legend, the reader is referred to the web version of this article.)

2.5. Synchronous and asynchronous 2T2D COS maps

The 2T2D COS algorithm, when applied to spectra, produces synchronous and asynchronous maps. The auto-peaks are represented by
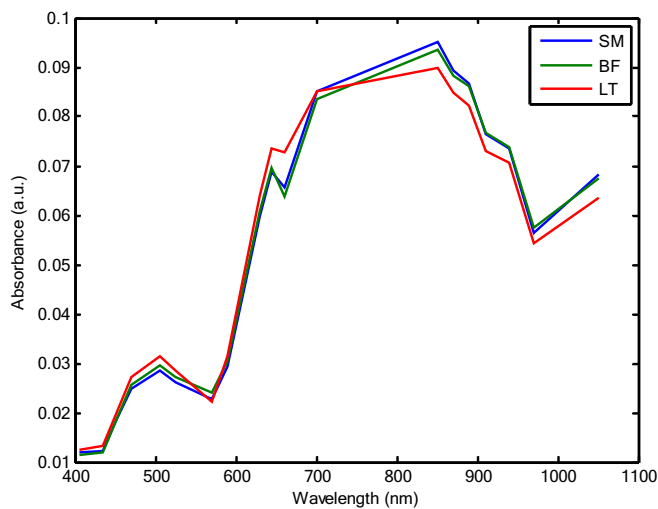
Fig. 3. Mean spectra of the three muscles; *Biceps femoris* (BF), *Longissimus thoracis* (LT), and *Semimembranosus* (SM) of the Blonde d'Aquitaine breed.

the diagonal line in the symmetric 2T2D synchronous map. The magnitude spectrum is produced by extracting the auto-peaks. Cross-peaks are peaks that are located off the map's diagonal. The cross-peaks, which are always positive, describe a similar pattern in spectral intensity

changes between the spectrum to be analyzed (ν) and the reference spectrum r(v). With regard to the diagonal line, the asynchronous map is asymmetric and only displays cross-peaks. Those cross-peaks indicate that two bands at the origin of this peak are originating from different sources. The sign of the cross-peak is also informative, if the sign of the cross-peak is positive, the intensity contribution of the moiety represented by the wavelength band 1 ($\nu 1$) is more abundant than that of the wavelength band 2 ($\nu 2$) in s(ν) compared to the r(ν), and vice versa (Noda, 2018, 2022). The 2T2D COS maps were calculated by using MATLAB R2013b (The Mathworks Inc., Natic, MA, USA) on unprocessed mean spectra and on processed (i.e SNV, MSC, and AREA) spectra. The reference spectrum r(ν) used to calculate the maps was the respective mean spectrum of each class (i.e. muscle class considered: BF, LT or SM) and the sample of each muscle was considered as the sample spectrum s (ν). The asynchronous and synchronous maps were obtained using eqs. 1 and 2 respectively.

$$\psi(v_1, v_2) = \frac{1}{2}[s(v_1).r(v_2) - r(v_1).s(v_2)] \tag{1}$$

$$\phi(v_1, v_2) = \frac{1}{2}[s(v_1).s(v_2) + r(v_1).r(v_2)] \tag{2}$$

2.6. Principal components analysis

Principal Component Analysis (PCA) is a well-established technique in the literature. PCA calculates principal components, which are new
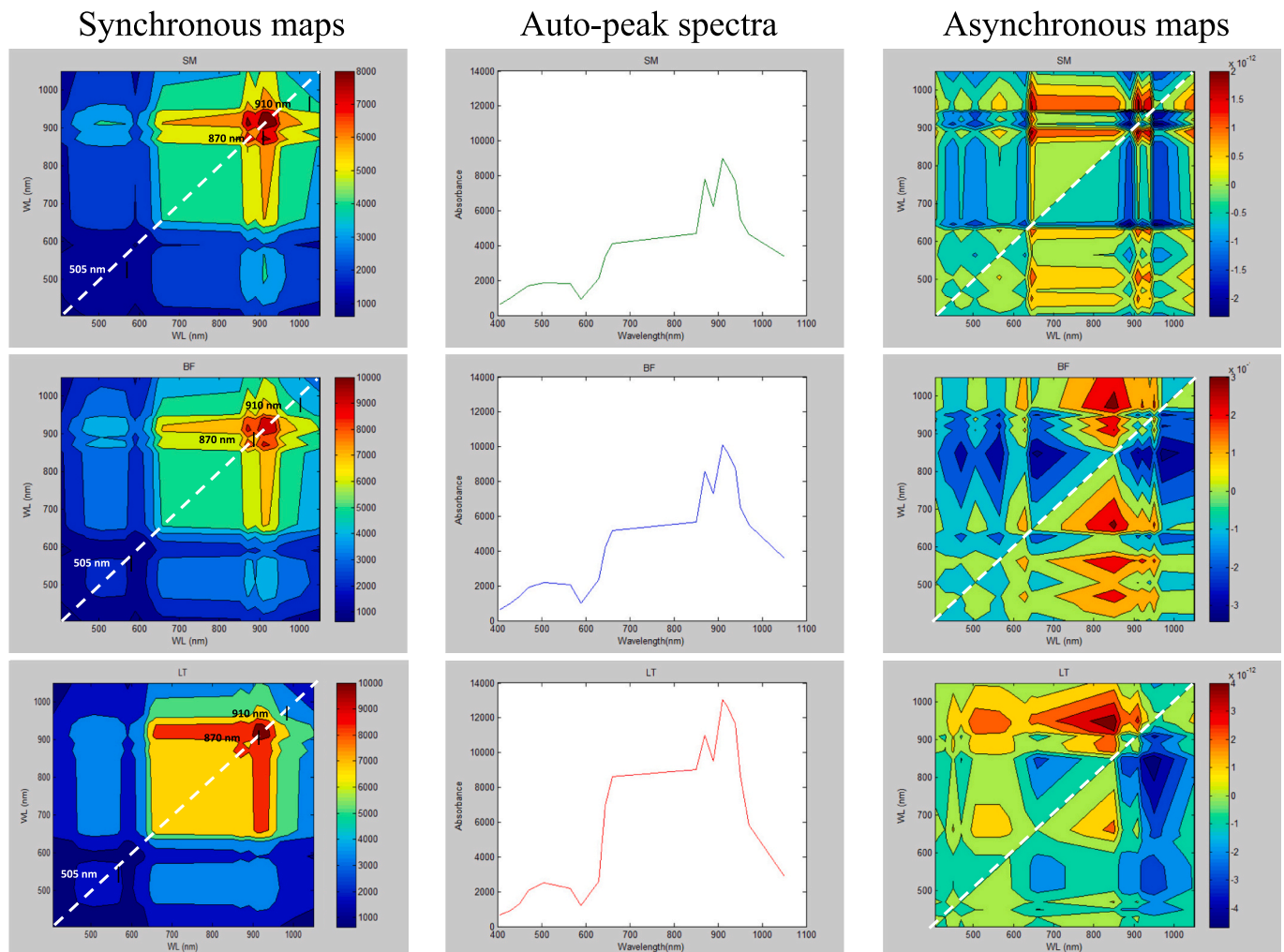

Fig. 4. Mean of synchronous and asynchronous 2TD2 COS maps of animal muscles, *Biceps femoris* (BF), *Longissimus thoracis* (LT), and *Semimembranosus* (SM).

orthogonal factors that represent the variance of the original data in a few dimensions (Jolliffe, 2002; Mishra et al., 2017; Vidal, Ma, & Sastry, 2005; Wang & Du, 2000). This technique was used to analyze MSI spectra and 2T2D COS data extracted from each muscle images. Due to the 3D data structure of the 2T2D COS maps $240 \times 19 \times 19$ (number of samples $\times$ number of wavelengths in the x-axis $\times$ number of wavelengths in the y-axis), these data have been unfolded before PCA. Unfolded data matrix was submitted to PCA to derive the first 19 principal components and examine the grouping of samples and ensure that the maximum of information was extracted from the initial data. Before data analysis and interpretation, the PCA loadings were folded back to give matrices similar to the initial data set. All the unfolding and folding steps were performed on MATLAB R2013b (The Mathworks Inc., Natic, MA, USA) by using our own command lines. Cross validation was performed by using the venetian blinds with 10 splits and 1 sample per split. Venetian Blinds is performed by building a model with 90% of the initial dataset and sub-validating the initial model by using the remaining 10% subset. Up until all datasets have been employed as a sub-validating subset, this phase is iteratively repeated. To estimate the model's performance on unknown data, the model's average result is computed (Nee, Bryan, Levitskaia, Kuo, & Nilsson, 2018). Before PCA analysis the MSI spectra and 2T2D COS maps were mean centered or auto-scaled. The PCA was performed with MATLAB R2013b (The Mathworks Inc., Natic, MA, USA) by using the PLS-Toolbox v.7.5 software (Eigenvector Research).

2.7. Partial least square discriminant analysis

The objective of PLS-DA is to predict the membership of an individual to a qualitative group that has been preliminarily defined. PLS-DA was used to develop models for distinguishing between muscle types. Therefore, before performing PLS-DA, spectra of meat samples were divided into three classes of muscles (BF, LT, and SM). PLS-DA was performed on four data matrices. The first PLS-DA was performed on the MSI mean spectra after subtracting the average spectra from each MSI mean spectra data (normalization by mean centering). Mean centering was performed with MATLAB R2013b (The Mathworks Inc., Natic, MA, USA). The second PLS-DA was applied to the 2T2D COS synchronous maps. The third PLS-DA models were built after considering the 2T2D COS asynchronous maps and the last PLS-DA models were obtained after concatenating the data matrix of 2T2D COS synchronous and

asynchronous maps.

The entire set of samples was randomly split into three data sets in order to assess the performance of the model: 60% of the samples were used for model calibration, 20% were used for model validation, and 20% were used to test the accuracy of the model. Each sample class (calibration, validation, and testing) was defined by using the *dividerand* function (with values for *trainRatio:0.6, valRatio:0.2,* and *testRatio:0.2*) proposed in MATLAB R2013b (The Mathworks Inc., Natic, MA, USA). All the PLS-DA models were performed in MATLAB R2013b (The Mathworks Inc., Natic, MA, USA) by using the PLS-Toolbox v.7.5 (Eigenvector Research Inc., Manson, WA, USA). The accuracy (how often the classification model is correct overall), recall (what proportion of actual positives was identified correctly?), and precision (the ratio of correctly classified positive samples to a total number of classified positive samples - either correctly or incorrectly-) parameters were calculated by using eqs. 3, 4, and 5. The adjustment of the performance and regression factors (Loading Vector) of the PLS-DA models were evaluated by analyzing the error of each model obtained after the model-testing step.

$$accuracy\ (\%) = \frac{TP + TN}{TP + TN + FP + FN} \times 100 \tag{3}$$

$$recall\ (\%) = \frac{TP}{TP + FN} \times 100 \tag{4}$$

$$precision\ (\%) = \frac{TP}{TP + FP} \times 100 \tag{5}$$

TP = True positive (samples belonging to the modelled class, if they are correctly predicted to be inside the boundary of that class); FP = False positive (when samples not belonging to the modelled class are incorrectly predicted to be inside the boundary of that class); TN = True negative (samples not belonging to the modelled class, if they are correctly predicted to be outside the boundary of that class); FN = False negative (samples belonging to the class being modelled are incorrectly predicted to be outside the boundary of that class).

3. Results and discussion

3.1. Spectral signature of the muscles

Fig. 3 presents the mean of the RAW spectra of the three muscles (BF,

Table 1
Bands coordinates identified on muscle asynchronous spectra (in green color: *Longissimus thoracis;* in blue color: *Semi membranosus;* in red color: *Biceps femoris).*

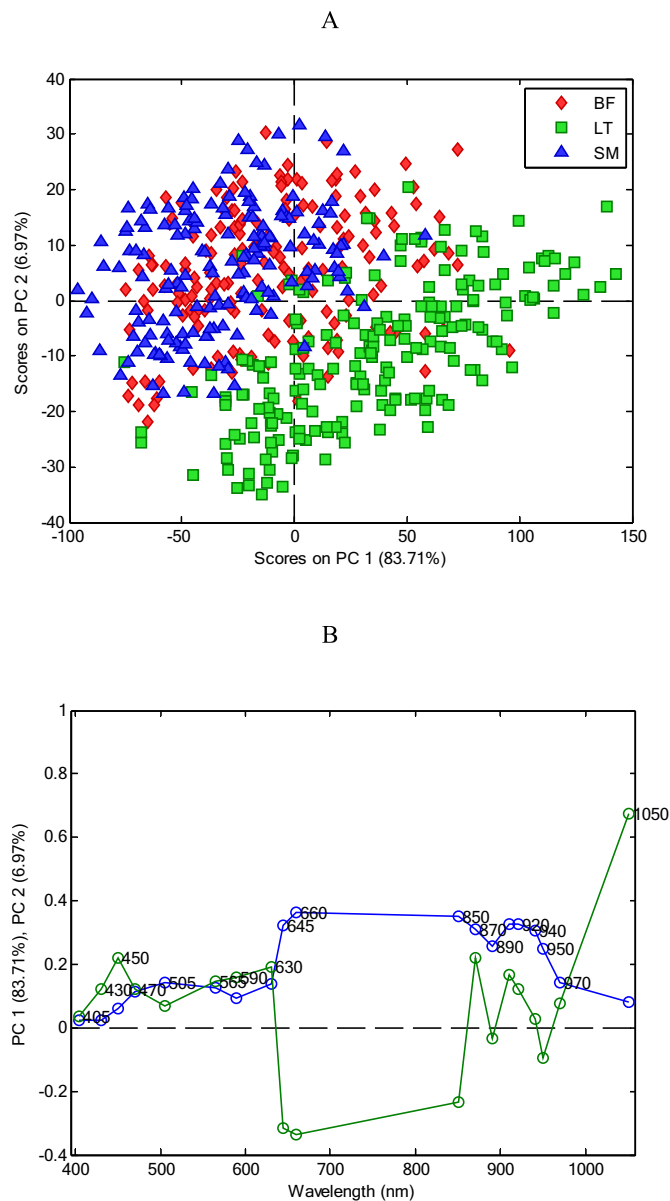|	Sign and position (in nm) of identified cross-peaks													
	450	470	505	565	590	630	645	660	850	890	910	920	940	950
565			(+)											
630		(+)		(-)(+)										
645	(+)		(+)			(+)								
660						(-)								
850		(+)(+)		(+)				(+)(+)						
870														
890				(-)			(-)							
900														
910	(+)		(+)			(+)(-)			(-)	(+)				
920			(+)				(-)				(-)			
940	(+)		(+)			(+)(-)			(-)	(+)				
950		(-)	(-)(+)	(-)		(-)		(+)	(-)		(-)(-)		(-)	
970			(-)			(-)	(-)		(-)		(-)	(-)		(-)

A

B

Fig. 5. Scores (A) and loadings (B) obtained after principal components analysis of MSI spectra. Blue line: PC1 loading; green line: PC2 loading). (For interpretation of the references to color in this figure legend, the reader is referred to the web version of this article.)

LT, and SM). Those spectra were described in detail in previous articles (Aït-Kaddour et al., 2020, 2017). The MSI spectra are very similar and no huge difference amongst them can be observed. Compared to previous papers (Aït-Kaddour et al., 2020, 2017), no clear difference can be pointed out. The current spectra exhibit a small reflectance band with a maximum at 500 nm, a shoulder at 645 nm, and a band with a maximum at 850 nm. However, slight differences amongst reflectance intensities of the bands can be observed. This certainly underlines differences in muscle physical (e.g. sensory tenderness, shear force) and chemical properties (e.g. Lipids, collagen, proteoglycan) as previously reported (Dubost et al., 2013; Dubost, Micol, Meunier, et al., 2013). Indeed, the absorption bands in the wavelength range studied (405–1050 nm) are due to the stretching of chemical bonds such as O—H, C—H, or N—H of organic molecules (Sanz et al., 2016). The 405–600 nm region is related to muscles pigment (Cozzolino, Barlocco, Vadell, Ballesteros, & Gallieta, 2003; Davis, Birth, & Townsend, 1978; Franke & Solberg, 1971; Isdell, Allen, Doherty, & Butler, 2003; Liu et al., 2003; Prieto, López-Campos,

Zijlstra, Uttaro, & Aalhus, 2014; Swatland, 1983; Torrescano, Sanchez-Escalante, Gimenez, Roncales, & Beltrán, 2003). Swatland (1989) also associated the slope shape observed between 600 and 700 nm to the formation of oxymyoglobin. The 775–850 nm range can be related to the N—H vibration of proteins (Mitsumoto, Maeda, Mitsuhashi, & Ozawa, 1991; Peng & Wang, 2015). From 850 to 950 nm there is the third overtone C—H stretching (Peng & Wang, 2015). The region from 950 to 1100 nm was reported as sensitive to the second overtone of N—H and O—H stretching (Peng & Wang, 2015). Therefore, the band at 940 nm can be related to meat fat and the 1050 nm band to both fat and/or proteins (Osborne, 2006; Šašić & Ozaki, 2000; Workman Jr, 1996).

3.2. Description of the 2T2D COS maps

The mean of synchronous and asynchronous 2T2 DCOS maps calculated on raw spectra of the different muscles are presented in Fig. 4. In the synchronous map, it can be observed that muscle category gave the same landscape with peaks maxima located at 505, 870, and 910 nm (Fig. 4, auto-peak spectra). Based on previous research, the band located at 505 nm can be assigned to metmyoglobin or meat pigment (Cozzolino & Murray, 2004; Mitsumoto et al., 1991). The 870 and 910 nm bands can be related to protein vibrations (Lu et al., 2020) and the band located at 890 nm was associated to water (O—H bonds) (Andrés et al., 2007). This showed the presence of abundant protein, water, and metmyoglobin in meat sample as generally reported. The comparison of the auto-peak spectra revealed that band maxima intensities varied from one muscle class to another. The intensities of the bands decreased in the following order, LT, BF, and SM. This could suggest differences in concentration of proteins, water, and metmyoglobin in the LT, BF and SM muscle class as previously reported (Kim, Yang, & Jeong, 2016; Rickansrud & Henrickson, 1967).

In the asynchronous map, the number of cross-peaks and their smaller area indicates a marked similarity between the two samples that are compared. The asynchronous maps of the three muscle types presented differences in both quantity and shape of cross-peaks (Fig. 4, asynchronous map). The number of cross-peaks identified were 6, 24, and 17 for LT, SM, and BF muscles maps, respectively (Table 1). This suggested that higher similarity between breeds could be found in LT muscles class, followed by BF muscles class, and finally SM muscles class. This might be due to the fact that the LT muscle contained less collagen, lipids, cross-links, cross-links per mole of collagen compared to the two other muscles, as revealed in the previous studies (Dubost, Micol, Meunier, et al., 2013; Dubost, Micol, Picard, et al., 2013). In addition, the LT muscle is the one with the most homogeneous perimysium and endomysium (in length, width, and degree of ramification) compared to the three muscles previously studied (Dubost, Micol, Meunier, et al., 2013). This could explain why the results of the present study showed a higher similarity between breeds for LT muscle.

The sign of the cross-peaks can be analyzed to assess the presence or absence of molecular vibrations in relation to the mean spectrum (i.e. reference spectrum). When the cross-peak has a negative sign, it means that the control sample has more of the detected molecular vibration than the examined sample, and vice versa. Fig. 4 shows that the signs of the cross-peaks (negative or positive) depend on the muscle considered. From the cross-peaks coordinates reported in Table 1, it can be suggested that differences between muscles and the reference spectrum can be due to differences in the muscle color, composition, and molecular structure. These suggested certainly a variability in chemical composition into the same muscle class. This difference in muscle classes can be due to the difference in muscle development of each animal. Late-maturing cattle breeds such as LI and BA deposit more muscle and less fat, compared to early-maturing cattle breeds, such as AA. The muscles of breeds such as AA contain more collagen (Christensen et al., 2011; Dubost, Micol, Meunier, et al., 2013) and have more oxidative but less glycolytic metabolism. These results suggested that 2T2D COS maps could be a good data management strategy to discriminate muscle types.

3.3. Results of principal components analysis

Fig. 5 shows the score plot and the associated loading of the first two principal components (PC1 vs PC2) derived from the raw MSI spectra. The first PC described 83.71% of variance, while the second PC described 6.97% of variance. The clustering between LT and BF/SM muscles can be observed along the PC1 axis. Based on the loading profile of PC1, highest contributing wavelengths for the separation between LT and BF/SM were observed between 645 nm to 950 nm for PC1. This region was associated to oxymyoglobin (Swatland, 1989), N—H
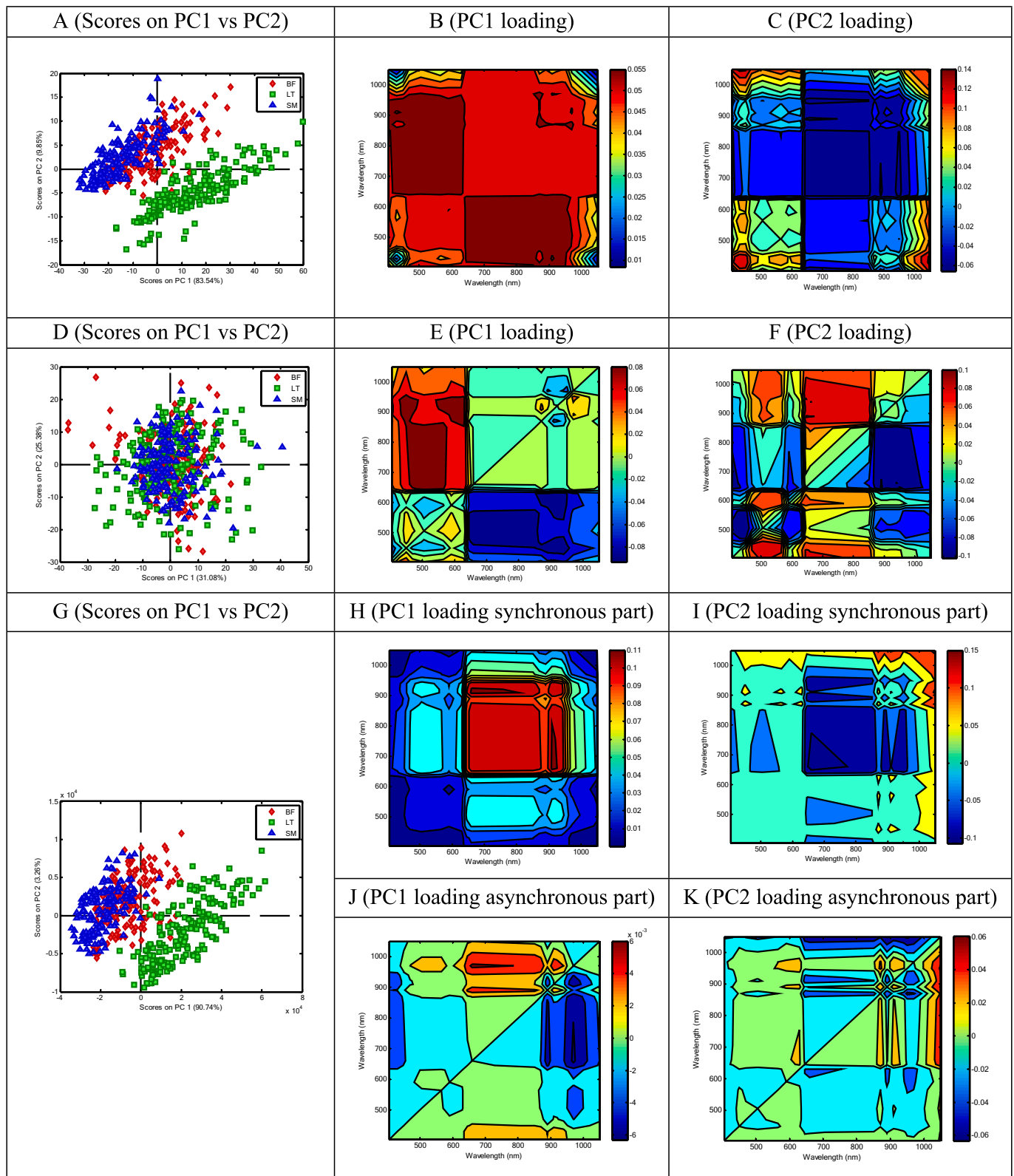

Fig. 6. Scores (A, D, G) and loading of PC1 and PC2 obtained after principal components analysis of 2T2D COS synchronous maps (A, B, C), asynchronous maps (D, E, F) and after combining 2T2D COS synchronous and asynchronous maps (G, H, I, J, K).

vibration of proteins (Mitsumoto et al., 1991; Peng & Wang, 2015), and C—H stretching (Peng & Wang, 2015).

Fig. 6 presents scores plots and loadings associated to the 2 first principal components obtained after PCA analysis of synchronous, asynchronous and the combination of synchronous and asynchronous maps. When compared to the MSI spectra results, we can notice a slightly better discrimination amongst muscles regardless the strategy adopted (e.g. analysis of synchronous map alone or analysis of the combination of synchronous and asynchronous map). However, the general trend in the scores map was preserved. This confirms the assumption that different spectral attributes between samples are associated with characteristics of the muscles depending on their type and that 2T2D COS method provides more specific information associated to each muscle. When considering the synchronous map alone or the combination of synchronous and asynchronous maps, a clustering can be observed, along the PC1 axis, between the LT and BF/SM muscles. Moreover, the amount of the total data variance explained by the PC1 was 83.71%, when considering the synchronous map, and 90.74% when considering the analysis of the combination of synchronous and asynchronous maps. As observed in Fig. 6D, no clustering between beef muscles was observed after PCA analysis of the asynchronous maps. Therefore, only the PC1 of the synchronous and combination of synchronous and asynchronous maps will be considered further.

Based on the PC1 loading profile (Fig. 6B), and of the auto-peak spectra (i.e. diagonal line of the PC1 loading) obtained after analysis of the synchronous maps it can be observed that LT muscles, when compared to BF/SM, presented higher values for all the wavelengths except for the 430 nm (muscles pigment), 450 nm (muscles pigment) and 1050 nm (fat and/or proteins) wavelengths. Those three wavelengths presented low intensity (< 0.01 a.u.) when compared to the other bands intensities (> 0.04 a.u.). All those factors can explain the clustering observed between BF/SM and LT muscles.

PCA results obtained after analysis of the combination of synchronous and asynchronous maps highlighted different wavelength bands regions that were important for data clustering. For PC1 loading of the synchronous part, bands in the 645–850 nm range (oxymyoglobin and N—H of proteins) and bands located at 890 nm (O—H bonds) and 920 nm (fat vibrations) contributed mostly to the data clustering. In this region, the LT muscles presented the highest intensity, while the other two muscles (BF/SM) presented the lowest one. For the asynchronous part, the cross-peaks contributing mostly to discrimination were observed at different wavelength coordinates reported in the Table 2. Six negative bands located at different coordinates (405 vs 630 to 950; 590 vs 470 to 565; 890 vs 630 to 870; 970 vs 470 to 590; 970 vs 645 to 870 and 970 vs 920) and one positive band at the coordinates (920 vs 890) were identified in the PC1 loading, suggesting that those regions are important for muscles discrimination. Positive area refers to positive correlation, indicating a group of absorption bands change simultaneously (either stronger or weaker), while negative area is just the reverse.

Table 2
Spectral bands coordinates identified on the PC1 loading map obtained after PCA analysis of the combination of synchronous and asynchronous maps of the different beef muscles.

	x – axis (cm^{-1})	y – axis (cm^{-1})	Sign of the cross peak
Band 1	405	630 to 950	(−)
Band 2	590	470 to 565	(−)
Band 3	890	630 to 870	(−)
Band 4	920	890	(+)
Band 5	970	470 to 590	(−)
Band 6	970	645 to 870	(−)
Band 7	970	920	(−)

3.4. Partial Least Squares Discrimination analysis

3.4.1. Results of the PLSDA models

Table 3 summarizes the best PLS-DA models results (number of optimal loading vector (LV), model error, percentage of accuracy, recall, and precision) of muscle classification carried out on MSI mean spectra, synchronous maps, asynchronous maps, and the combination of synchronous and asynchronous maps. It can be observed that MSI spectra presented results for error, accuracy, precision, and recall ranging between 15.40 and 21.60, 71.30–82.41, 70.76–90.90, and 70.90–81.34%, respectively. Those results were built using between 2 and 10 LV. The highest error after testing the model was obtained with the AREA preprocessing (21.60%), followed by MSC preprocessing (18.60%), then by considering RAW data (15.70%) and finally the data corrected by SNV (15.40%). Concerning the accuracy, precision and recall factors, the highest values were obtained with the SNV preprocessing (81.48, 80.99, and 81.34%, respectively), then with data corrected by the AREA preprocessing (78.70, 76.86, and 77.40%, respectively), followed by RAW data (74.07, 72.53, and 72.70%, respectively), and finally after correcting the data by the MSC preprocessing (72.22, 70.76, and 71.78%, respectively). Therefore, it can be pointed out that the model providing the best classification factors and lowest error, for the test step, was obtained after correcting the MSI spectra by the SNV method. Accordingly, the application of SNV preprocessing before performing PLS-DA on MSI spectra is strongly advised.

For training, validation, and testing, the calculated PLS-DA models with the synchronous maps presented error, accuracy, precision, and recall varying from 5.50 to 9.80, 89.81–92.52, and 88.83–91.15, 88.47–91.04%, respectively. As noted with the MSI spectra, the highest error after testing the model was also obtained with the AREA preprocessing (9.80%), while the data corrected by SNV gave the lowest error (5.50%). Equivalent classification errors were obtained when considering the RAW data (error = 7.20%) or data corrected by MSC (error = 7.10%). Concerning the accuracy, precision, and recall factors, the highest factors were obtained with the MSC preprocessing (92.59, 91.15, 90.48%, respectively), then by the SNV preprocessing (90.74, 90.61, 91.04%, respectively), and followed by AREA (90.74, 90.00, 90.36%, respectively) preprocessing. Finally, the lowest classification factors were obtained when the data were not preprocessed (89.81, 88.83, 88.47%, respectively). From these results, it can be concluded that the best model after testing was obtained with the SNV preprocessing method because this one gives the lowest error (error of the test = 5.50%) and the most parsimonious model due to the lowest number of LV used (i.e. 6).

Compared to the PLS-DA model obtained by considering the MSI spectra, we can observe that the synchronous transformation provided a significant improvement of the model performance (i.e. error with MSI spectra = 15.40% and error for synchronous spectra = 5.50%). Therefore, it is advisable to use synchronous map after 2T2D COS transformation of MSI spectra before performing PLS-DA in order to increase the model discrimination performance.

When considering the asynchronous maps and regardless of training, validation, and test, the accuracy, precision and recall ranged between 35.19 and 63.89%, 34.42–63.28%, and 34.72–62.63%, while the error varied from 23.80 to 48.00%. The best model was obtained when the PLS-DA received the data after AREA preprocessing. This model was calculated with 6 LV and exhibited outputs of 23.80, 63.89, 62.86, and 62.36% for error, accuracy, precision, and recall, respectively. It can be pointed out that using the asynchronous maps for performing discrimination gave very unsatisfactory results and that using asynchronous map after 2T2D COS transformation of MSI spectra before muscle discrimination is not advisable. This is certainly associated to the noisy shape of the asynchronous map and the low intensity exhibited by the asynchronous bands.

All the PLS-DA models exhibited a level of 100% for the entire classification factors when considering both synchronous and

Table 3
PLSDA factors (error, accuracy, precision and recall) in percentage of the best discrimination models calculated for beef muscles discrimination.

		LV	Calibration				Validation				Test			
			Error	Accuracy	Precision	Recall	Error	Accuracy	Precision	Recall	Error	Accuracy	Precision	Recall
MSI Spectra	RAW	8	13.70	78.95	78.44	78.49	19.60	81.48	78.47	78.73	15.70	74.07	72.53	72.70
	SNV	10	14.30	78.95	76.92	76.99	15.70	71.30	90.90	70.90	15.40	81.48	80.99	81.34
	MSC	10	14.30	79.61	78.58	78.68	19.60	82.41	80.61	80.55	18.60	72.22	70.76	71.78
	AREA	2	16.00	78.22	77.32	77.54	17.60	76.85	74.58	74.35	21.60	78.70	76.86	77.40
Asyn	RAW	1	44.30	48.22	50.07	47.49	48.00	43.52	45.08	42.22	43.00	40.74	43.50	40.38
	SNV	1	42.10	54.05	54.26	52.33	47.90	35.19	34.42	34.72	46.40	38.89	40.17	38.54
	MSC	10	34.30	54.37	57.05	54.40	33.90	45.37	46.31	48.04	29.30	44.44	41.71	42.61
	AREA	6	27.90	63.19	63.28	62.63	33.70	58.33	57.02	57.44	23.80	63.89	62.86	62.36
Syn	RAW	10	5.60	90.85	90.79	90.82	9.70	88.89	43.50	86.94	7.20	89.81	88.83	88.47
	SNV	6	6.70	94.74	94.03	94.03	12.60	90.74	40.17	90.43	5.50	90.74	90.61	91.04
	MSC	10	5.30	90.52	90.06	90.03	5.20	89.81	41.71	89.55	7.10	92.59	91.15	90.48
	AREA	8	5.40	94.08	93.46	93.46	8.30	90.74	62.86	90.32	9.80	90.74	90.00	90.36
Asyn + Syn	RAW	10	0.00	100	100	100	0.00	100	100	100	0.00	100	100	100
	SNV	10	0.00	100	100	100	0.00	100	100	100	0.00	100	100	100
	MSC	6	0.00	100	100	100	1.40	100	100	100	0.00	100	100	100
	AREA	6	0.00	100	100	100	0.50	100	100	100	0.00	100	100	100

RAW: raw spectra; SNV: spectra after standard normal variate preprocessing; MSC: spectra after multiple scattering preprocessing; AREA: spectra after normalization of the area under the curve to a value of 1; Asyn: Asynchronous map; Syn: synchronous map; Asyn + Syn: concatenated synchronous and asynchronous maps; LV: loading vector.

asynchronous maps. The number of LV used for calculating the models varied from 6 to 10 depending on the preprocessed method (i.e. SNV, MSC, or AREA). For testing, accurate results were obtained after preprocessing spectra with MSC or AREA methods due to the low number of LV (i.e. 6) needed to build the discrimination model. Therefore, when considering the combination of synchronous and asynchronous maps, the usage of MSC or AREA preprocessing can be advised to combine parsimony of the model and the highest classification factors for beef muscles discrimination. Achieving such high-performance in discrimination is undoubtedly related to the complementarity exiting between the two maps.

The present results indicate that the three studied muscles could be classified perfectly using MSI combined with 2T2D COS-PLS-DA. When compared to the literature, the present models are outperforming the ones previously published by Sanz et al. (2015) and Aït-Kaddour et al. (2017) using respectively HSI and MSI. These results are also outperforming those reported with other spectral techniques, like fluorescence spectroscopy (Aït-Kaddour, Loudiyi, Ferlay, & Gruffat, 2018; Frencia, Thomas, & Dufour, 2003; Sahar & Dufour, 2015). As for them, Sahar and Dufour (2015) reported 100% of correct classification for three beef muscles (*Infraspinatus*, *Rectus abdominus*, and *Semitendinosus*) with the 290 nm excitation wavelength. However, contrary to the present study, their analyses were investigated on only one breed, the heifers Charolais.

3.4.2. Effect of preprocessing on the model performance

Prior to conducting additional analysis, most of the time spectra are corrected to increase the differences between groups, to linearize the response of the variables, and remove irrelevant variations. In most chemometric analyses, preprocessed data were found to provide higher classification accuracy compared to raw data. However, it is generally hard to predict in advance what preprocessing will give the best modeling outcomes. Thus, three processing approaches—SNV, MSC, and AREA—were investigated in order to evaluate the impact of the preprocessing quality on the model discrimination performance. Our findings demonstrate that preprocessing typically enhances classification performance. The best classification model accuracy was obtained when applying the SNV transformation to MSI spectra and synchronous maps, while models calculated with asynchronous data gave the best classification features after AREA transformation. However, the models were not satisfactory. SNV attempts at making all spectra comparable in terms

of intensities (or absorbance level). It can be useful to correct spectra for changes in optical path length and light scattering (it is assumed that the standard deviation of the spectra represents well these changes). SNV is, for example, frequently used to compensate for changes in surface roughness of the material (Sandak et al., 2016) that can be useful in differentiation beef muscles based on their surface texture as noted in Fig. 1 and reported by Aït-Kaddour et al. (2017). Therefore, those factors can explain why SNV can be recommended before analyzing such data. The concatenation of asynchronous and synchronous maps gave the best discrimination outcomes when MSC and AREA preprocessing were used. In fact, compared to models obtained using either the SNV transformation approach (i.e., 10) or no transformation (i.e., RAW data), those models required less LV (i.e., 6). The huge difference in intensity between the synchronous (1000 to 10,000 a.u.) and asynchronous (-4 to 4×10^{-12} a.u.) maps, and the need to reduce this variability, may explain why MSC and AREA are more adequate for providing the best predictive models (Dieterle et al., 2006; Windig et al., 2008).

4. Conclusion

In this study, we evaluated the applicability of PLS-DA coupled with MSI data (spectra, 2T2D COS synchronous and asynchronous maps) to discriminate three beef muscles. Discrimination of muscles was performed successfully with high classification accuracy and low prediction error after testing the model on new data. The results also highlighted the potential of 2T2D COS coupled with PLS-DA to increase the discrimination (100% for classification accuracy, precision, and recall and 0% for error) performance when compared to the models calculated by using directly MSI spectra without any transformation.

These results revealed that the strategy of combining 2T2D COS - PLS-DA with MSI is a good way to reach high performance for discrimination. This study brings a new approach in the analysis of the MSI data allowing to reach interesting results in term of discrimination performance. Hence, we hope that this strategy can be implemented for routine analysis and respond to the increasing interest of the meat industry for online techniques to discriminate beef muscles.

CRediT authorship contribution statement

Abderrahmane Aït-Kaddour: Writing – review & editing, Writing – original draft, Visualization, Validation, Supervision, Software, Methodology, Investigation, Formal analysis, Data curation, Conceptualization. **Mohammed Loudiyi:** Writing – review & editing. **Oumayma Boukria:** Writing – review & editing. **Jasur Safarov:** Writing – review & editing. **Shaxnoza Sultanova:** Writing – review & editing. **Donato Andueza:** Writing – review & editing. **Anne Listrat:** Writing – review & editing, Writing – original draft, Resources, Funding acquisition. **Yana Cahyana:** Writing – review & editing.

Declaration of competing interest

The authors declare no conflict of interest.

Data availability

Data will be made available on request.

References

Aït-Kaddour, A., Andueza, D., Dubost, A., Roger, J.-M., Hocquette, J.-F., & Listrat, A. (2020). Visible and near-infrared multispectral features in conjunction with artificial neural network and partial least squares for predicting biochemical and Micro-structural features of beef muscles. *Foods, 9*(9), 1254.

Aït-Kaddour, A., Jacquot, S., Micol, D., & Listrat, A. (2017). Discrimination of beef muscle based on visible-near infrared multi-spectral features: Textural and spectral analysis. *International Journal of Food Properties, 20*(6), 1391–1403.

Aït-Kaddour, A., Loudiyi, M., Ferlay, A., & Gruffat, D. (2018). Performance of fluorescence spectroscopy for beef meat authentication: Effect of excitation mode and discriminant algorithms. *Meat Science, 137*, 58–66. https://doi.org/10.1016/J.MEATSCI.2017.11.002

Aït-Kaddour, A., Thomas, A., Mardon, J., Jacquot, S., Ferlay, A., & Gruffat, D. (2016). Potential of fluorescence spectroscopy to predict fatty acid composition of beef. *Meat Science, 113*, 124–131.

Andrés, S., Murray, I., Navajas, E. A., Fisher, A. V., Lambe, N. R., & Bünger, L. (2007). Prediction of sensory characteristics of lamb meat samples by near infrared reflectance spectroscopy. *Meat Science, 76*(3), 509–516.

Barnes, I., Bastian, V., Becker, K. H., & Martin, D. (1989). *Fourier Transform IR Studies of the Reactions of Dimethyl Sulfoxide with OH, NO3, and Cl Radicals, 3*, 476–488. https://doi.org/10.1021/bk-1989-0393.ch030

Casale, M., Casolino, C., Ferrari, G., & Forina, M. (2008). Near infrared spectroscopy and class modelling techniques for the geographical authentication of Ligurian extra virgin olive oil. *Journal of Near Infrared Spectroscopy, 16*(1), 39–47.

Christensen, M., Ertbjerg, P., Failla, S., Sañudo, C., Richardson, R. I., Nute, G. R., … Juárez, M. (2011). Relationship between collagen characteristics, lipid content and raw and cooked texture of meat from young bulls of fifteen European breeds. *Meat Science, 87*(1), 61–65.

Cozzolino, D., Barlocco, N., Vadell, A., Ballesteros, F., & Gallieta, G. (2003). The use of visible and near-infrared reflectance spectroscopy to predict colour on both intact and homogenised pork muscle. *LWT- Food Science and Technology, 36*(2), 195–202.

Cozzolino, D., & Murray, I. (2004). Identification of animal meat muscles by visible and near infrared reflectance spectroscopy. *LWT- Food Science and Technology, 37*(4), 447–452.

Davis, G. W., Birth, G. S., & Townsend, W. E. (1978). Analysis of spectral reflectance for measuring pork quality. *Journal of Animal Science, 46*(3), 634–638.

Dieterle, F., Ross, A., Schlotterbeck, G., & Senn, H. (2006). Probabilistic quotient normalization as robust method to account for dilution of complex biological mixtures. Application in ^{1} H NMR Metabonomics. *Analytical Chemistry, 78*(13), 4281–4290. https://doi.org/10.1021/ac051632c

Dubost, A., Micol, D., Meunier, B., Lethias, C., & Listrat, A. (2013). Relationships between structural characteristics of bovine intramuscular connective tissue assessed by image analysis and collagen and proteoglycan content. *Meat Science, 93*(3), 378–386.

Dubost, A., Micol, D., Picard, B., Lethias, C., Andueza, D., Bauchart, D., & Listrat, A. (2013). Structural and biochemical characteristics of bovine intramuscular connective tissue and beef quality. *Meat Science, 95*(3), 555–561.

Feng, C.-H., Makino, Y., Oshita, S., & Martín, J. F. G. (2018). Hyperspectral imaging and multispectral imaging as the novel techniques for detecting defects in raw and processed meat products: Current state-of-the-art research advances. *Food Control, 84*, 165–176.

Franke, W. C., & Solberg, M. (1971). Quantitative determination of metmyoglobin and total pigment in an intact meat sample using reflectance spectrophotometry. *Journal of Food Science, 36*(3), 515–519.

Frencia, J. P., Thomas, E., & Dufour, E. (2003). Measure of meat tenderness using front-face fluorescence spectroscopy. *Sciences des Aliments, 23*(1), 142–145.

Gowen, A. A., O'Donnell, C. P., Cullen, P. J., Downey, G., & Frias, J. M. (2007). Hyperspectral imaging–an emerging process analytical tool for food quality and safety control. *Trends in Food Science and Technology, 18*(12), 590–598.

Isdell, E., Allen, P., Doherty, A., & Butler, F. (2003). Effect of packaging cycle on the colour stability of six beef muscles stored in a modified atmosphere mother pack system with oxygen scavengers. *International Journal of Food Science and Technology, 38*(5), 623–632.

Jolliffe, I. T. (2002). *Principal component analysis for special types of data.* Springer.

Kamruzzaman, M., ElMasry, G., Sun, D.-W., & Allen, P. (2012). Non-destructive prediction and visualization of chemical composition in lamb meat using NIR hyperspectral imaging and multivariate regression. *Innovative Food Science & Emerging Technologies, 16*, 218–226.

Kim, G.-D., Yang, H.-S., & Jeong, J.-Y. (2016). Comparison of characteristics of myosin heavy chain-based fiber and meat quality among four bovine skeletal muscles. *Korean Journal for Food Science of Animal Resources, 36*(6), 819.

Kim, S. S., Rhyu, M., Kim, J. M., & Lee, S. (2003). Authentication of rice using near-infrared reflectance spectroscopy. *Cereal Chemistry, 80*(3), 346–349.

Listrat, A., Gagaoua, M., Andueza, D., Gruffat, D., Normand, J., Mairesse, G., Picard, B., & Hocquette, J.-F. (2020). What are the drivers of beef sensory quality using metadata of intramuscular connective tissue, fatty acids and muscle fiber characteristics? *Livestock Science, 240*, Article 104209.

Liu, Y., Lyon, B. G., Windham, W. R., Realini, C. E., Pringle, T. D. D., & Duckett, S. (2003). Prediction of color, texture, and sensory characteristics of beef steaks by visible and near infrared reflectance spectroscopy. A feasibility study. *Meat Science, 65*(3), 1107–1115.

Lu, Y., Wang, W., Huang, M., Ni, X., Chu, X., & Li, C. (2020). Evaluation and classification of five cereal fungi on culture medium using visible/near-infrared (Vis/NIR) hyperspectral imaging. *Infrared Physics & Technology, 105*, Article 103206.

Mishra, S. P., Sarkar, U., Taraphder, S., Datta, S., Swain, D., Saikhom, R., … Laishram, M. (2017). Multivariate statistical data analysis-principal component analysis (PCA). *International Journal of Livestock Research, 7*(5), 60–78.

Mitsumoto, M., Maeda, S., Mitsuhashi, T., & Ozawa, S. (1991). Near-infrared spectroscopy determination of physical and chemical characteristics in beef cuts. *Journal of Food Science, 56*(6), 1493–1496.

Moreirinha, C., Nunes, A., Barros, A., Almeida, A., & Delgadillo, I. (2015). Evaluation of the potential of mid-infrared spectroscopy to assess the microbiological quality of ham. *Journal of Food Safety, 35*(2), 270–275.

Nache, M., Scheier, R., Schmidt, H., & Hitzmann, B. (2015). Non-invasive lactate- and pH-monitoring in porcine meat using Raman spectroscopy and chemometrics. *Chemometrics and Intelligent Laboratory Systems, 142*, 197–205. https://doi.org/10.1016/j.chemolab.2015.02.002

Nee, K., Bryan, S. A., Levitskaia, T. G., Kuo, J. W.-J., & Nilsson, M. (2018). Combinations of NIR, Raman spectroscopy and physicochemical measurements for improved monitoring of solvent extraction processes using hierarchical multivariate analysis models. *Analytica Chimica Acta, 1006*, 10–21. https://doi.org/10.1016/j.aca.2017.12.019

Noda, I. (1993). Generalized two-dimensional correlation method applicable to infrared, Raman, and other types of spectroscopy. *Applied Spectroscopy, 47*(9), 1329–1336.

Noda, I. (2018). Two-trace two-dimensional (2T2D) correlation spectroscopy–a method for extracting useful information from a pair of spectra. *Journal of Molecular Structure, 1160*, 471–478.

Noda, I. (2022). Two-trace two-dimensional (2T2D) correlation applied to a number of spectra beyond a simple pair. *Spectrochimica Acta. Part A, Molecular and Biomolecular Spectroscopy, 277*, Article 121258. https://doi.org/10.1016/j.saa.2022.121258

Osborne, B. G. (2006). *Near-infrared spectroscopy in food analysis. Encyclopedia of Analytical Chemistry: Applications, Theory and Instrumentation.*

Panagou, E. Z., Papadopoulou, O., Carstensen, J. M., & Nychas, G.-J. E. (2014). Potential of multispectral imaging technology for rapid and non-destructive determination of the microbiological quality of beef filets during aerobic storage. *International Journal of Food Microbiology, 174*, 1–11. https://doi.org/10.1016/j.ijfoodmicro.2013.12.026

Peng, Y., & Wang, W. (2015). Application of near-infrared spectroscopy for assessing meat quality and safety. In *Infrared spectroscopy—Anharmonicity of biomolecules, Crosslinking of Biopolymers, Food Quality and Medical Applications.*

Pérez-Palacios, T., Caballero, D., Antequera, T., Durán, M. L., Ávila, M., & Caro, A. (2017). Optimization of MRI acquisition and texture analysis to predict Physico-chemical parameters of loins by data mining. *Food and Bioprocess Technology, 10*(4), 750–758. https://doi.org/10.1007/s11947-016-1853-4

Prieto, N., Andrés, S., Giráldez, F. J., Mantecón, A. R., & Lavín, P. (2006). Potential use of near infrared reflectance spectroscopy (NIRS) for the estimation of chemical composition of oxen meat samples. *Meat Science, 74*(3), 487–496.

Prieto, N., López-Campos, Ó., Zijlstra, R. T., Uttaro, B., & Aalhus, J. L. (2014). Discrimination of beef dark cutters using visible and near infrared reflectance spectroscopy. *Canadian Journal of Animal Science, 94*(3), 445–454.

Rao, M. S., Chakraborty, G., & Murthy, K. S. (2019). Market drivers and discovering technologies in meat species identification. *Food Analytical Methods, 12*(11), 2416–2429.

Rickansrud, D. A., & Henrickson, R. L. (1967). Total pigments and myoglobin concentration in four bovine muscles. *Journal of Food Science, 32*(1), 57–61.

Sahar, A., & Dufour, É. (2015). Classification and characterization of beef muscles using front-face fluorescence spectroscopy. *Meat Science, 100*, 69–72.

Sandak, A., Sandak, A., & Meder, R. (2016). Assessing trees, wood and derived products with near infrared spectroscopy: Hints and tips. *Journal of Near Infrared Spectroscopy, 24*(6), 485–505. https://doi.org/10.1255/jnirs.1255

Sanz, J. A., Fernandes, A. M., Barrenechea, E., Silva, S., Santos, V., Gonçalves, N., … Melo-Pinto, P. (2015). Lamb muscle discrimination using hyperspectral imaging:

Comparison of various machine learning algorithms. *Journal of Food Engineering, 174*, 92–100. https://doi.org/10.1016/j.jfoodeng.2015.11.024

Sanz, J. A., Fernandes, A. M., Barrenechea, E., Silva, S., Santos, V., Gonçalves, N., … Melo-Pinto, P. (2016). Lamb muscle discrimination using hyperspectral imaging: Comparison of various machine learning algorithms. *Journal of Food Engineering, 174*, 92–100.

Šašić, S., & Ozaki, Y. (2000). Band assignment of near-infrared spectra of milk by use of partial least-squares regression. *Applied Spectroscopy, 54*(9), 1327–1338.

Swatland, H. J. (1983). Infrared fiber optic spectrophotometry of meat. *Journal of Animal Science, 56*(6), 1329–1333.

Swatland, H. J. (1989). Carotene reflectance and the yellowness of bovine adipose tissue measured with a portable fibre-optic spectrophotometer. *Journal of the Science of Food and Agriculture, 46*(2), 195–200.

Tao, F., Peng, Y., Li, Y., Chao, K., & Dhakal, S. (2012). Simultaneous determination of tenderness and Escherichia coli contamination of pork using hyperspectral scattering technique. *Meat Science, 90*(3), 851–857. https://doi.org/10.1016/j.meatsci.2011.11.028

Torrescano, G., Sanchez-Escalante, A., Gimenez, B., Roncales, P., & Beltrán, J. A. (2003). Shear values of raw samples of 14 bovine muscles and their relation to muscle collagen characteristics. *Meat Science, 64*(1), 85–91.

Vidal, R., Ma, Y., & Sastry, S. (2005). Generalized principal component analysis (GPCA). *IEEE Transactions on Pattern Analysis and Machine Intelligence, 27*(12), 1945–1959.

Wang, F.-K., & Du, T. C. T. (2000). Using principal component analysis in process performance for multivariate data. *Omega, 28*(2), 185–194.

Wei, W., Peng, Y., Li, Y., & Qiao, L. (2015, July 26). *Lightweight portable nondestructivedetection technique for assessing meat freshness attributes based on light emitting diode array. 2015 ASABE international meeting.* https://doi.org/10.13031/aim.20152189624

Windig, W., Shaver, J., & Bro, R. (2008). Loopy MSC: A simple way to improve multiplicative scatter correction. *Applied Spectroscopy, 62*(10), 1153–1159. https://doi.org/10.1366/000370208786049097

Workman, J. J., Jr. (1996). Interpretive spectroscopy for near infrared. *Applied Spectroscopy Reviews, 31*(3), 251–320.